physica status solidi b
www.pss-b.com
basic solid state physics

Energy loss of swift H and He projectiles in Al, Si, Ni and Cu targets

Cristian D. Denton[1], Isabel Abril[1], Juan Carlos Moreno-Marín[2], Santiago Heredia-Avalos[2], and Rafael Garcia-Molina[3]

[1] Departament de Física Aplicada, Universitat d'Alacant, Apartat 99, 03080 Alacant, Spain
[2] Departament de Física, Enginyeria de Sistemes i Teoria del Senyal, Universitat d'Alacant, Apartat 99, 03080 Alacant, Spain
[3] Departamento de Física – CIOyN, Universidad de Murcia, Apartado 4021, 30080 Murcia, Spain

Received 9 July 2007, revised 16 April 2008, accepted 13 May 2008
Published online 24 June 2008

PACS 34.50.Bw, 61.80.Jh, 77.22.–d

We have calculated the stopping power of Al, Si, Ni and Cu for swift H and He ion beams. Furthermore, the energy loss straggling corresponding to Ni is also evaluated. The dielectric formalism is used combined with the MELF-GOS method, which describes the energy loss function of the target by a linear combination of Mermin type energy loss functions for the electron outer-shell electrons and by generalized oscillator strengths for the electron inner-shell electrons. We take into account the corrections to the stopping power associated to capture and loss of electrons by the projectile as well as the polarization of the projectile charge density. The versatility of this method is illustrated by the good agreement between their predictions and the experimental results, which is observed for a wide range of projectile energies and targets with different electronic properties.

phys. stat. sol. (b) **245**, No. 8, 1498–1504 (2008) / **DOI** 10.1002/pssb.200743283

phys. stat. sol. (b) **245**, No. 8, 1498–1504 (2008) / **DOI** 10.1002/pssb.200743283

physica status solidi b
www.pss-b.com
basic solid state physics

Energy loss of swift H and He projectiles in Al, Si, Ni and Cu targets

Cristian D. Denton[*,1], Isabel Abril[1], Juan Carlos Moreno-Marín[2], Santiago Heredia-Avalos[2], and Rafael Garcia-Molina[3]

[1] Departament de Física Aplicada, Universitat d'Alacant, Apartat 99, 03080 Alacant, Spain
[2] Departament de Física, Enginyeria de Sistemes i Teoria del Senyal, Universitat d'Alacant, Apartat 99, 03080 Alacant, Spain
[3] Departamento de Física – CIOyN, Universidad de Murcia, Apartado 4021, 30080 Murcia, Spain

Received 9 July 2007, revised 16 April 2008, accepted 13 May 2008
Published online 24 June 2008

PACS 34.50.Bw, 61.80.Jh, 77.22.–d

[*] Corresponding author: e-mail denton@ua.es, Fax: +34 965 90 97 26

We have calculated the stopping power of Al, Si, Ni and Cu for swift H and He ion beams. Furthermore, the energy loss straggling corresponding to Ni is also evaluated. The dielectric formalism is used combined with the MELF-GOS method, which describes the energy loss function of the target by a linear combination of Mermin type energy loss functions for the electron outer-shell electrons and by generalized oscillator strengths for the electron inner-shell electrons. We take into account the corrections to the stopping power associated to capture and loss of electrons by the projectile as well as the polarization of the projectile charge density. The versatility of this method is illustrated by the good agreement between their predictions and the experimental results, which is observed for a wide range of projectile energies and targets with different electronic properties.

1 Introduction The knowledge of the stopping power of a material, defined as the mean energy loss of a projectile per unit path length, has multiple technological applications in several areas such as microelectronics, material analysis, protection against radiation or radiation therapy [1–3].

The excitation of target electrons by a swift projectile is the main mechanism that contributes to the stopping power in the energy range we are considering here ($E > 10$ keV/u), and hence the electronic properties of the material determine the energy loss of the projectiles. There is a lot of experimental data in the bibliography about the inelastic stopping power for swift projectiles in solids for different projectile-target combinations [4]. Several models have been developed to explain and predict these experimental results [5], from the pioneering works by Bohr [6], Bethe [7], and Bloch [8] to the most recent ones [9–13].

The behavior of some materials, such as the transition metals, which have a broad excitation spectrum, can not be treated as a free electron gas and requires a more realistic description [13]. Our model [13–18] allows to obtain the electronic energy loss of swift light ion beams in solids (either elemental targets or compounds) using the dielectric formalism. In this scheme the response of the target electrons due to the perturbation produced by the projectile is obtained by the MELF-GOS (Mermin Energy Loss Functions combined with Generalized Oscillator Strenghts) model. This method consists in fitting the experimental optical data corresponding to the target outer-shell electrons by a linear combination of Mermin-type [19] energy loss functions and to describe the response of the inner-shell electrons by generalized oscillator strengths [20]. On the other hand, the projectile electronic charge density is included here using hydrogen-like wave functions. We take into account the polarization of the projectile electron cloud due to the self-induced electric field [21]. The possible charge states the projectile can acquire inside the solid, and the stopping power due to capture and loss of electrons by the projectile are also considered.

The energy loss of light ions in elemental (Ge, Fe, Ti . . .) and compounds (GaAs, SiC, LiF . . .) targets has already been evaluated [13, 15–17]. Similar calculations were carried out and reported previously for H ions in Al, Si and Cu [14], but in addition, we now take into account

the different charge states the projectile can acquire when moving through the target, the energy loss associated to the electronic capture and loss processes, and the polarization of the projectile [13, 21].

Here we check the reliability of our model in obtaining the stopping power of materials with different electronic properties by comparing our calculations with the available experimental results.

In Section 2 we introduce the model we use to obtain the stopping power and the energy loss straggling of a material and the main results are presented in Section 3. Finally the conclusions of our work are presented in Section 4.

2 Model

2.1 Charge state approach to the stopping power Once a projectile penetrates a material it begins to capture and lose electrons until charge equilibrium is reached in a few femtoseconds. The stopping power of the material, S_p, depends on the projectile charge state, then we can calculate S_p as a sum of the partial stopping powers $S_{p,q}$ due to each charge state q,

$$S_p = \sum_{q=0}^{Z_1} \phi_q S_{p,q} \,, \tag{1}$$

where ϕ_q is the fraction of the projectiles with the q charge state when charge equilibrium is reached, which depends on the target, the projectile atomic number Z_1 and its velocity v. We use the values of ϕ_q provided by the CasP 3.1 code [22].

In a similar way, the energy loss straggling Ω^2, defined as the variance in the energy lost by the projectile per unit path length, can also be expressed as a sum of partial stragglings Ω_q^2 for each projectile charge state q.

2.2 Dielectric description of the stopping parameters In order to calculate $S_{p,q}$ and Ω_q^2 we use the dielectric formalism, which is based on a linear response of the stopping medium to the perturbation produced by the projectile charge density [23]. Within this scheme we write:

$$S_{p,q} = \frac{2e^2}{\pi v^2} \int_0^{\infty} \frac{\mathrm{d}k}{k} \left[Z_1 - \rho_q(k) \right]^2 \int_0^{kv} \mathrm{d}\omega\, \omega\, \mathrm{Im}\left[\frac{-1}{\varepsilon(k,\omega)} \right], \tag{2}$$

where e is the elementary charge, $\hbar k$ and $\hbar\omega$ are, respectively, the momentum and energy transferred to the target electrons, $\hbar$ is Planck's constant, $\rho_q(k)$ is the Fourier transform of the projectile electronic density for the q charge state, and $\mathrm{Im}\,[-1/\varepsilon(k,\omega)]$ is the energy loss function of the target. We can improve the predictions of Eq. (2) by considering that the electron cloud of a dressed projectile is displaced a distance d_q from the nucleus due to the effect of the self-induced electric field. This polarization effect gives rise to a correction in the stopping power $S_{pol,q}$ [21], which must be added to the previous equation of $S_{p,q}$,

$$S_{pol,q}(v) = \frac{2e^2 Z_1}{\pi v^2} \int_0^{\infty} \frac{\mathrm{d}k}{k}\, \rho_q(k) \int_0^{kv} \mathrm{d}\omega\, \omega \times \mathrm{Im}\left[\frac{-1}{\varepsilon(k,\omega)} \right] \left[1 - \cos\left(\frac{\omega d_q}{v} \right) \right]. \tag{3}$$

We use $d_q = \alpha_q\, E_q(v)$, where α_q is the projectile polarizability and $E_q(v)$ is the self-induced electric field produced by the projectile, given by

$$E_q(v) = \frac{2e}{\pi v^2} \int_0^{\infty} \frac{\mathrm{d}k}{k} \left[Z_1 - \rho_q(k) \right] \int_0^{kv} \mathrm{d}\omega\, \omega\, \mathrm{Im}\left[\frac{-1}{\varepsilon(k,\omega)} \right]. \tag{4}$$

The corresponding expressions for the partial energy loss straggling, Ω_q^2, are similar to Eqs. (2) and (3), but replacing $\hbar\omega$ by $(\hbar\omega)^2$.

In our calculations we have obtained the electronic charge density ρ_q from hydrogenic wave functions, but taking into account the dynamic screening due to the target electrons, as stated in Ref. [21]. In the case of neutral He, we consider the additional screening of the interaction between the nucleus and its electrons using an effective nuclear charge given by Slater's rules [24].

2.3 MELF-GOS description of the ELF The main ingredient to obtain the stopping power and the energy loss straggling is the energy loss function (ELF) of the target, and therefore a good model for the ELF is the key of a suitable description of the energy loss. The ELF determines the probability that an inelastic event with momentum transfer $\hbar k$ and energy transfer $\hbar\omega$ takes place in the target, and contains information about the electronic excitations that the material can sustain. Within the MELF-GOS model, the ELF is described by separating the contribution to the target electronic excitations coming from outer- and inner-shell electrons. The contribution of the formers to the ELF is obtained by fitting the experimental ELF in the optical limit ($k = 0$) by a linear combination of Mermin-type ELF [13, 14],

$$\mathrm{Im}\left[\frac{-1}{\varepsilon(k=0,\omega)} \right]_{\mathrm{outer}} = \sum_i A_i\ \mathrm{Im}\left[\frac{-1}{\varepsilon_M(\omega_i,\gamma_i;k=0,\omega)} \right]_{\omega \geq \omega_{th,i}}, \tag{5}$$

with ε_M being a Mermin-type dielectric function [19]. The fitting parameters ω_i and γ_i are related, respectively, with the position and the width of the peaks observed in the ELF, while the coefficients A_i determine their relative weight; $\omega_{th,i}$ is a threshold energy. One of the advantages of this method is that the ELF is analytically extended to all values of $\hbar k$ through the properties of the Mermin dielectric function [25]. Although the experimental data of the ELF for $k \neq 0$ are very scarce or even non-existent, we have

obtained in aluminum and graphite a more accurate description of the excitation spectra for $k \neq 0$ when using our MELF-GOS model than when using other ELF models [25].

On the other side the description of the contribution to the ELF of the inner-shell electrons is done in terms of the generalized oscillator strengths (GOS) for isolated atoms; this approach is suitable since inner-shell electrons have large binding energies and show negligible collective effects. The relation between the ELF and the GOS is given by [20]

$$\mathrm{Im}\left[\frac{-1}{\varepsilon(k,\omega)}\right]_{\mathrm{inner}} = \frac{2\pi^2 N}{\omega}\sum_{n\ell}\frac{\mathrm{d}f_{n\ell}(k,\omega)}{\mathrm{d}\omega}, \qquad (6)$$

where N is the atomic density of the target and $\mathrm{d}f_{n\ell}(k,\omega)/\mathrm{d}\omega$ is the GOS of the (n, ℓ) subshell. The summation is extended over all inner subshells of the target atoms that retain their atomic character. Of course, the ionization of a given subshell can only take place if the energy transfer $\hbar\omega$ is larger than a threshold energy $\hbar\omega_{n\ell}$. We employ the GOS in the hydrogenic approach because it gives realistic values of the inner-shell ionization cross-sections and provides analytical expressions for inner-shell ionizations [15, 18].

For the fitting to be satisfactory, the resulting ELF must verify the f-sum rule, that is, the effective number of excited electrons per atom when $\hbar\omega \to \infty$ must tend to the total number of electrons per atom [26]. Moreover, we obtain a good agreement between our calculated mean excitation energy I and the experimental data [27] of each target.

The optical limit of the ELF for Al, Si, Ni and Cu is depicted in Fig. 1. The solid lines represent our fitted ELF,

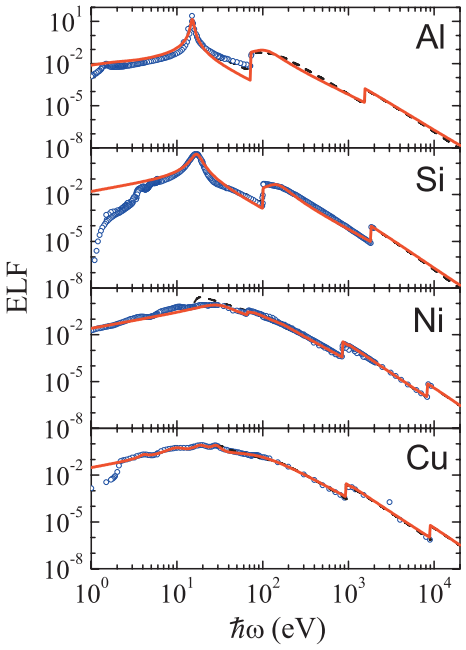

Figure 1 (online colour at: www.pss-b.com) Energy loss functions of Al, Si, Ni and Cu, in the optical limit ($k = 0$), as a function of the excitation energy $\hbar\omega$. Solid lines represent our model, symbols are experimental data [28] and dashed lines are obtained from the X-ray scattering factors [29].

Table 1 Parameters used to fit the outer-shell electrons contribution to the optical ELF of Al, Si, Ni and Cu. N is the atomic density of the target.

target, N	i	$\hbar\omega_{\mathrm{th},i}$ (eV)	$\hbar\omega_i$ (eV)	γ_i (eV)	A_i
Al,	1		15.0	0.95	1.0
6.03×10^{22} at/cm^3	2	72.5	106.1	81.6	6.7×10^{-2}
Si,	1		16.87	4.24	9.92×10^{-1}
5.00×10^{22} at/cm^3	2	99.8	146.93	95.23	2.74×10^{-2}
Ni,	1		31.56	32.65	7.43×10^{-1}
9.13×10^{22} at/cm^3	2	66.12	78.91	40.82	8.38×10^{-2}
	3		93.06	149.11	1.16×10^{-1}
	4		163.26	76.19	6.67×10^{-3}
Cu,	1		4.08	1.09	2.0×10^{-2}
8.49×10^{22} at/cm^3	2		10.07	5.99	2.18×10^{-1}
	3		19.05	8.16	2.45×10^{-1}
	4		27.21	8.16	1.52×10^{-1}
	5		78.91	152.38	3.56×10^{-1}

with the parameters corresponding to the outer electron excitations (see Eq. (5)) given in Table 1. The symbols correspond to experimental data of the ELF [28], and the dashed lines were obtained from experimental X-ray scattering factors [29]. It is interesting to discuss the behaviour of the differents ELFs. In the case of Al a sharp peak in the plasma frequency denotes the behaviour of a material with quasi free electrons in the valence band. The silicon target has a broader peak because plasmon excitation has a larger lifetime and can decay more easily into other excitations. Ni and Cu have much more complex ELFs that cannot be accounted for with a free electron gas description and involve interband transitions. For this reason we have used only two Mermin-type energy loss functions to fit the ELF of Al and Si, and 4 or 5 functions for the more complex materials. The K-shell of Al and Si is described by a GOS as well as the K and L-shells of Ni and Cu. Although the fitting function departs from the experiments at very low excitation energies, this part of the spectra does not contribute very much to the stopping power or energy loss straggling.

Using these ELF representations in the corresponding expressions for $S_{p,q}$ and Ω_q^2, we calculate the main momenta of the electronic energy loss distribution, namely the stopping power and the energy loss straggling, which will be presented in Section 3.

2.4 Stopping power and energy loss straggling associated to capture and loss processes The process of charge changing of the projectile involves an energy loss that can be a significative correction to the stopping power in a certain energy range. If only processes of capture and loss of a single electron are considered, the stopping power due to capture and loss events can be described as [30]

$$S_{\mathrm{C\&L}} = N\sum_{q=0}^{Z_1-1}\phi_q\sigma_{q\to q+1}U_{q\to q+1} + \phi_{q+1}\sigma_{q+1\to q}U_{q+1\to q}, \qquad (7)$$

$\sigma_{q\to q+1}$ being the electron loss cross section and $\sigma_{q+1\to q}$ the electron capture cross section. $U_{q\to q+1}$ and $U_{q+1\to q}$ are the energy transferred in the loss and capture processes, respectively. When charge equilibrium has been reached it is verified that

$$\phi_q\ \sigma_{q\to q+1} = \phi_{q+1}\ \sigma_{q+1\to q}\ , \tag{8}$$

and Eq. (7) can be rewritten as

$$S_{\mathrm{C\&L}} = N \sum_{q=0}^{Z_1-1} \phi_q\ \sigma_{q\to q+1}\,[U_{q\to q+1} + U_{q+1\to q}]\,. \tag{9}$$

The energy lost by the projectile in a capture and loss cycle, $\Delta E_{\mathrm{C\&L}}$, can be approximated by

$$\Delta E_{\mathrm{C\&L}} = [U_{q\to q+1} + U_{q+1\to q}] \approx \tfrac{1}{2} m_{\mathrm{e}} v^2 + E_t\ , \tag{10}$$

where m_{e} is the electron mass and E_t is the first ionization energy of the target atom [31].

For the evaluation of the electron loss cross sections $\sigma_{q\to q+1}$ we have assumed the same model proposed by Brandt and Sizmann (BS) for hydrogen [32, 33]. In the case of helium projectiles we assume that the electron loss cross section is proportional to the number of projectile K-shell electrons, n_{K}, and to the effective area of the projectile. Therefore the generalized BS cross section results

$$\sigma_{q\to q+1} = n_{\mathrm{K}}(\pi r_{\mathrm{at}}^2)\left(\frac{2}{3}\right)^2\left(\frac{Z_2^{2/3}}{Z_2^{2/3}+v}\right)\left[\frac{4Z_2^{1/3}(Z_2+1)}{4Z_2^{1/3}(Z_2+1)+v}\right], \tag{11}$$

where Z_2 is the target atomic number, $r_{\mathrm{at}} = 3/(2Z_1)$ is the mean radius of the projectile and Z' is the effective nuclear charge given by Slater's rules [24]; of course $Z_1' = Z_1$ for hydrogenic atoms.

The electronic capture and loss events contribute to the energy loss straggling mainly due to the variation of the stopping power for the different charge states of the projectile [34]. We have estimated this contribution using a simulation code which has been described before [16, 35]. In our code the projectile moving with a given charge state slows down with a stopping power given by Eq. (2). In order to get only the contribution of the energy loss straggling due the variation of the partial stopping powers we set to zero the intrisic straggling of each charge state. Then we obtain the projectile energy distributions using our simulation code. In this way, the width of these energy distributions provide the energy loss straggling due only to the different charge states the projectile can acquire, i.e. the main contribution to the energy loss straggling associated to electronic capture and loss processes.

3 Results We represent in Figs. 2 and 3 the calculated stopping cross section SCS (SCS = S_{N}) for H and He ions in Al, Si, Ni and Cu, using Eqs. (1) and (2), and including both corrections due to polarization of the projectile and charge exchange events represented by the solid blue lines. For comparison purposes, we have plotted as dashed red

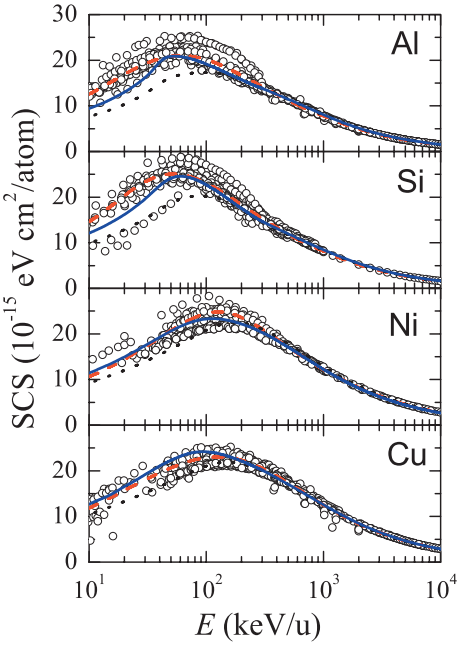

Figure 2 (online colour at: www.pss-b.com) Electronic stopping cross section (SCS) for H projectiles in Al, Si, Ni and Cu. The solid blue lines are our calculations, the dashed red lines are the SRIM [36] results, the dotted black lines are the results considering an average charge state for the projectile. Experimental data [4] are represented by symbols.

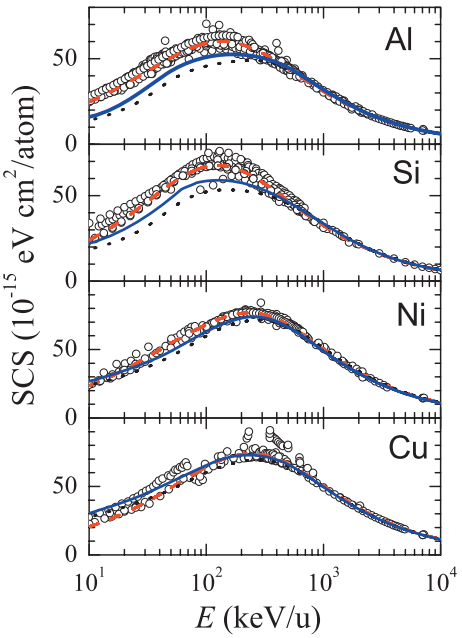

Figure 3 (online colour at: www.pss-b.com) Electronic stopping cross section (SCS) for He projectiles in Al, Si, Ni and Cu. The solid blue lines are our calculations, the dashed red lines are the SRIM [36] results, the dotted black lines are the results considering an average charge state for the projectile. Experimental data [4] are represented by symbols.

lines the semiempirical predictions of the SRIM-2008 code [36], which are based on fits to experimental stopping cross sections. The symbols correspond to a compilation of the available experimental data [4]. The dotted black lines are the results obtained when considering an average charge state for the projectile according to the charge states obtained from the CasP 3.1 code [22].

It is worth to emphasize the good agreement of our model with the experimental data for such a variety of target electronic properties (from a free electron gas metal as Al, to a complex one such as Ni or Cu, and a semiconductor like Si) and in a wide range of projectile energies. This is due, mainly, to an appropriate description of the target ELF. However, discrepancies between theory and experiment appear at low energies, because our calculations are based on the dielectric formalism, which assumes a linear response of the target electrons to the perturbation induced by the projectile. The dielectric formalism loses validity as the perturbation grows, i. e., when the projectile has high charge and low energy. In this situation non-linear effects, such as the Bloch and Barkas corrections [37], become more significant. Bloch correction is negative and decreases SCS, whereas Barkas correction, which is the responsible of proton–antiproton SCS asymmetry, increases the SCS. Therefore, even though the dielectric formalism provides a reasonable good agreement for a wide range of projectile energies, it is not applicable for low projectile energies. In these cases the Binary Theory (BT) proposed in Ref. [12], the Unitary Convolution Approximation (UCA) described in Ref. [11], the Transport Cross Section (TCS) calculations presented in Ref. [10], or the more elaborate Density Functional Theory (DFT) could be used [9, 38]. However, these models also have constraints. BT includes the Barkas and Bloch corrections, although is generally applied for heavy projectiles ($Z_1 \geq 3$) in selected materials [12]. UCA can be used in principle for whatever projectile-target combination, but it does not take into account the Barkas correction and fails when the target has a broad excitation spectrum, like transition metals [11]. The non-perturbative TCS calculations include the Barkas and Bloch corrections and can be applied for any projectile, but the target is treated as a free electron gas [10]. DFT can be only used for very low projectile energies [9, 38]. The interested reader can consult the recent review by Arista and Lifschitz [39] on non-linear approaches to the energy loss of ions in solids or the ICRU report 2005 [40].

On the other hand the results obtained when considering an average charge state instead of the model presented in this work show greater discrepancies from experiments at energies near or lower the SCS maximum.

In order to evaluate the influence of the different contributions to the SCS, we present in Fig. 4 the total SCS of

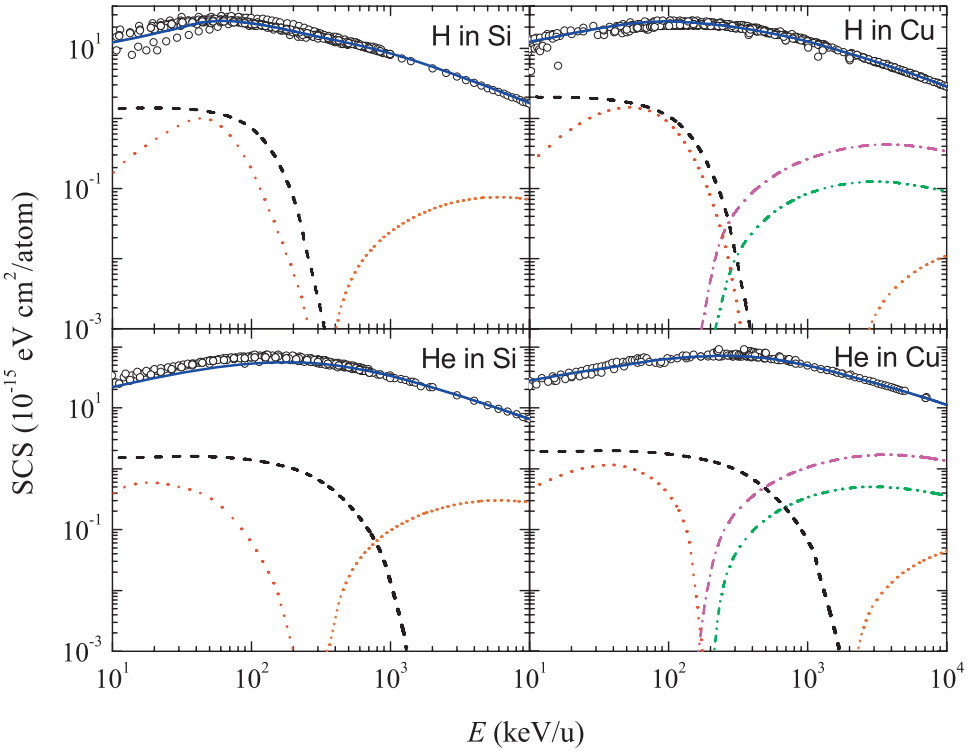

Figure 4 (online colour at: www.pss-b.com) Electronic stopping cross section (SCS) for H and He in Si (left panel) and Cu (right panel). The solid lines represent the total SCS while the discontinued lines are the minor contributions to the SCS, namely $S_{C\&L}$ (– – –), S_{pol} (·····), inner-shell contributions: 2p (–·– pink lines), 2s (–··– green lines), 1s (short dashed orange lines). Symbols are experimental data [4].

Si and Cu for H and He projectiles together with the contribution of the inner-shells, polarization of the projectile and electron capture and loss events. In the case of H projectiles, we observe that $S_{C\&L}$ contributes as much as 10% of the total SCS for Si and 15% for Cu at lower energies, where mostly charge changing events take place. On the other hand the polarization effect contribute to a maximum of 6% mainly at low energies. In the case of He projectiles these contributions are even smaller. Both contributions fade away at higher energies where the projectiles are fully stripped and represent a minor contribution to the total SCS, only being appreciable near or before the maximum of the SCS curve. Therefore a more accurate description of such processes would only result in imperceptible differences with our calculations.

The excitation of inner-shell electrons begins to be relevant at projectile energies high enough in order that the excitation energy exceeds the binding energy of the inner-shell electrons. At 10^4 keV/u they represent a 4% of the total SCS for Si and 15% for Cu.

The energy loss straggling of Al, Si and Cu for H and He has already been published [41], hence here we only show the results for the Ni target. In Fig. 5 we can see the energy loss straggling for H and He ions in Ni, normalized to the Bohr straggling $\Omega_B^2 = 4\pi N Z_1^2 Z_2$, as a function of the projectile energy. The black solid lines represent our calculations and the grey solid lines are the results obtained when considering an average charge for the projectile, while the symbols are experimental data from Refs. [42–48]. We can see a good agreement in the case of H projectiles for the whole energy range, whereas a less satisfactory agreement appears for He. The lack of experimental data and the difficulty in obtaining the experimental straggling can explain these discrepancies, especially if we consider that the energy loss straggling is experimentally overvalued due to factors such as roughness or inhomogeneity of the sample [41]. Considering or not the charge state of the projectile do not affect much the calculations of the energy loss straggling. Our results for Ω^2 shows the well-known tendency of the (Ω^2/Ω_B^2) ratio to unity at high projectile energies, however they are bound below Ω_B^2 in the whole energy range in opposition to some experimental data [44]. The contribution of the inner shells, represented by the dashed lines, is only relevant at high energies, being about 32% of the total Ω^2 at projectiles energies of 10^4 keV/u. The contribution to the straggling coming from charge exhange events is negligible for hydrogen projectiles. Nevertheless, for helium projectiles, the contribution of this term to the total straggling can be as high as 10% for projectile energies of 200 keV/u. Finally, the polarization effect in Ω^2 is very small and could be neglected.

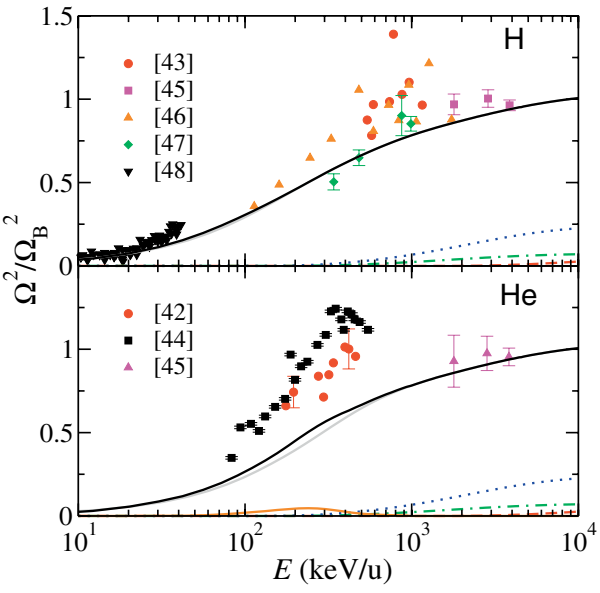

Figure 5 (online colour at: www.pss-b.com) Energy loss straggling for H and He in Ni as a function of the projectile energy normalized to the Bohr straggling. Black solid lines represent our results, grey solid lines are our calculations considering an average charge state for the projectile and symbols correspond to the available experimental data [42–48]. The discontinuous lines are the contribution of the inner shells, namely 1s (– – – red lines), 2s (–·– green lines) and 2p (····· blue lines). The contribution coming from the charge exchange processes for helium projectiles is the small hill appearing at ~200 keV/u (orange line).

4 Conclusions We present a calculation of the stopping power of Al, Si, Ni and Cu for H and He projectiles using the dielectric formalism together with the MELF-GOS method to describe the response of the target electrons to the perturbation produced by the projectile. We also take into account the charge states of the projectile inside the target, the effect of the polarization of the projectile and the contribution to the energy loss of the electron exchange events. The results agree reasonably well with experiments in all the targets analyzed here, showing that the MELF-GOS description is adequate for free electron gas materials like Al or more complex ones like Ni and Cu.

In addition, we have used the same method to obtain the energy loss straggling of Ni for H and He projectiles, obtaining also a reasonably good agreement with the available experiments, especially for H projectiles. The contribution of the inner-shells and capture and loss events is also established.

Acknowledgements This work was supported by the Spanish Ministerio de Educación y Ciencia (projects FIS2006-13309-C02-01 and FIS2006-13309-C02-02). CDD thanks the Spanish Ministerio de Educación y Ciencia and Generalitat Valenciana for support under the Ramón y Cajal Program and Universitat d'Alacant for support under project GRE07-1P.

References

[1] S. A. Campbell, The Science and Engineering of Microelectronic Fabrication (Oxford University, Oxford, 1996).
[2] M. Prutton, Electronic Properties of Surfaces (Adam Hilger, Bristol, 1984).

[3] J. Turner, Atoms, Radiation and Radiation Protection (Wiley, New York, 1995).
[4] H. Paul, Experimental stopping power compilation, available at http://www.exphys.uni-linz.ac.at/Stopping/
[5] P. Sigmund, Stopping of Heavy Ions (Springer, Berlin, 2004).
[6] N. Bohr, Philos. Mag. **25**, 10 (1913).
[7] H. Bethe, Ann. Phys. (Leipzig) **5**, 324 (1930).
[8] F. Bloch, Ann. Phys. (Leipzig) **16**, 285 (1933).
[9] M. Peñalba, J. I. Juaristi, E. Zarate, A. Arnau, and P. Bauer, Phys. Rev. A **64**, 012902 (2001).
[10] N. R. Arista, Nucl. Instrum. Methods Phys. Res. B **193**, 8 (2002).
[11] P. L. Grande, Nucl. Instrum. Methods Phys. Res. B **195**, 55 (2002).
[12] P. Sigmund and A. Schinner, Nucl. Instrum. Methods Phys. Res. B **195**, 64 (2002).
[13] S. Heredia-Avalos, R. Garcia-Molina, J. M. Fernández-Varea, and I. Abril, Phys. Rev. A **72**, 052902 (2005).
[14] I. Abril, R. Garcia-Molina, C. D. Denton, F. J. Pérez-Pérez, and N. R. Arista, Phys. Rev. A **58**, 357 (1998).
[15] S. Heredia-Avalos, J. C. Moreno-Marín, I. Abril, and R. Garcia-Molina, Nucl. Instrum. Methods Phys. Res. B **230**, 118 (2005).
[16] R. Garcia-Molina, I. Abril, C. D. Denton, and S. Heredia-Avalos, Nucl. Instrum. Methods Phys. Res. B **249**, 6 (2006).
[17] J. C. Moreno-Marín, I. Abril, S. Heredia-Avalos, and R. Garcia-Molina, Nucl. Instrum. Methods Phys. Res. B **249**, 29 (2006).
[18] I. Abril, J. C. Moreno-Marín, J. M. Fernández-Varea, C. D. Denton, S. Heredia-Avalos, and R. Garcia-Molina, Nucl. Instrum. Methods Phys. Res. B **256**, 172 (2007).
[19] N. D. Mermin, Phys. Rev. B **1**, 2362 (1970).
[20] R. F. Egerton, Electron Energy Loss Spectroscopy in the Electron Microscope (Plenum Press, New York, 1989).
[21] S. Heredia-Avalos and R. Garcia-Molina, Nucl. Instrum. Methods Phys. Res. B **193**, 15 (2002).
[22] P. L. Grande and G. Schiwietz, CasP. Convolution approximation for swift Particles, version 3.1 (2004) code available from http://www.hmi.de/people/schiwietz/casp.html.
[23] J. Lindhard, K. Dan. Vidensk. Selsk. Mat.-Fys. Medd. **28**, 8 (1954).
[24] J. C. Slater, Phys. Rev. **36**, 57 (1930).
[25] D. J. Planes, R. Garcia-Molina, I. Abril, and N. R. Arista, J. Electron Spectrosc. Relat. Phenom. **82**, 23 (1996).
[26] E. Shiles, T. Sasaki, M. Inokuti, and D. Y. Smith, Phys. Rev. B **22**, 1612 (1980).
[27] ICRU Report 49, Stopping Powers and Ranges for Protons and Alpha Particles (International Commission on Radiation Units and Measurements, Bethesda, 1993).
[28] E. D. Palik and G. Ghosh (eds.), The Electronic Handbook of Optical Constants of Solids (Academic Press, San Diego, 1999).
[29] B. L. Henke, E. M. Gullikson, and J. C. Davis, At. Data Nucl. Data Tables **54(**2) (1993).
and http://xray.uu.se/hypertext/henke.html.
[30] A. Arnau, Nucl. Instrum. Methods B **93**, 195 (1994).
[31] J. E. Huheey, E. A. Keiter, and R. L. Keiter, Inorganic Chemistry: Principles of Structure and Reactivity (Harper Collins, New York, 1993).
[32] W. Brandt and R. Sizmann, Atomic Collisions in Solids, Vol. 1 (Plenum Press, New York, 1975), p. 305.
[33] A. Chateau-Tierry, A. Gladieux, and B. Delaunay, Nucl. Instrum. Methods **132**, 553 (1976).
[34] T. Kaneko, Phys. Rev. A **33**, 1653 (1986).
[35] S. Heredia-Avalos, R. Garcia-Molina, and I. Abril, Phys. Rev. A **76**, 012901 (2007).
[36] J. F. Ziegler and J. P. Biersack, SRIM-2008. The Stopping and Range of Ions in Matter, Version 2008, code available from http://www.srim.org.
[37] J. C. Ashley, J. Phys.: Condens. Matter **3**, 2741 (1991).
[38] J. I. Juaristi, A. Arnau, P. M. Echenique, C. Auth, and H. Winter, Phys. Rev. Lett. **82**, 1048 (1999).
[39] N. R. Arista and A. F. Lifschitz, Adv. Quantum Chem. **45**, 47 (2004).
[40] A. Wambersie, P. M. DeLuca, Jr., and S. M. Seltzer, J. ICRU **5**, 21 (2005).
[41] C. C. Montanari, J. E. Miraglia, S. Heredia-Avalos, R. Garcia-Molina, and I. Abril, Phys. Rev. A **75**, 022903 (2007).
[42] J. M. Harris and M. A. Nicolet, Phys. Rev. B **11**, 1013 (1975).
[43] E. Friedland and J. M. Lombaard, Nucl. Instrum. Methods **163**, 523 (1979).
[44] E. Friedland and J. M. Lombaard, Nucl. Instrum. Methods **168**, 25 (1980).
[45] F. Besenbacher, J. U. Andersen, and E. Bonderup, Nucl. Instrum. Methods **168**, 1 (1980).
[46] J. M. Lombaard, J. Conradie, and E. Friedland, Nucl. Instrum. Methods **216**, 293 (1983).
[47] Y. Kido, Phys. Rev. B **34**, 73 (1986).
[48] H. H. Andersen, A. Csete, T. Ichioka, H. Knudsen, S. P. Møller, and U. I. Uggerhøj, Nucl. Instrum. Methods Phys. Res. B **194**, 217 (2002).

